WL-TR-95-4019

PROCESS OPTIMIZATION THROUGH
DISCOVERY AND INTEGRATION OF MATERIALS AND
PROCESSING PROPERTIES
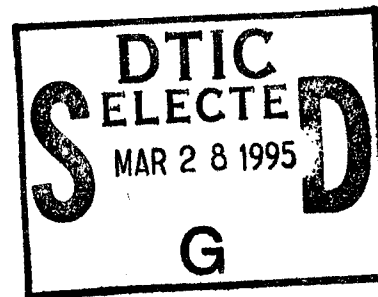
PERCY YIP

AI WARE, INC
1100 CEDAR AVE
CLEVELAND OH 44106

JANUARY 1995

FINAL REPORT FOR 07/01/94-12/31/94

DTIC
SELECTED
MAR 2 8 1995
G

APPROVED FOR PUBLIC RELEASE; DISTRIBUTION IS UNLIMITED.

MATERIALS DIRECTORATE
WRIGHT LABORATORY
AIR FORCE MATERIEL COMMAND
WRIGHT PATTERSON AFB OH 45433-7734

19950327 071

DTIC QUALITY INSPECTED 1

NOTICE

WHEN GOVERNMENT DRAWINGS, SPECIFICATIONS, OR OTHER DATA ARE USED FOR ANY PURPOSE OTHER THAN IN CONNECTION WITH A DEFINITE GOVERNMENT-RELATED PROCUREMENT, THE UNITED STATES GOVERNMENT INCURS NO RESPONSIBILITY OR ANY OBLIGATION WHATSOEVER. THE FACT THAT THE GOVERNMENT MAY HAVE FORMULATED OR IN ANYWAY SUPPLIED THE SAID DRAWINGS, SPECIFICATIONS, OR OTHER DATA, IS NOT TO BE REGARDED BY IMPLICATION, OR OTHERWISE IN ANY MANNER CONSTRUED, AS LICENSING THE HOLDER, OR ANY OTHER PERSON OR CORPORATION; OR AS CONVEYING ANY RIGHTS OR PERMISSION TO MANUFACTURE, USE, OR SELL ANY PATENTED INVENTION THAT MAY IN ANY WAY BE RELATED THERETO.

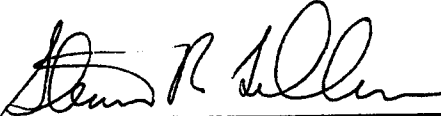## LICENSE RIGHTS LEGEND

Contract Number: F33615-94-C-5805
Contractor: AI WARE, Incorporated

This technical report has been reviewed and is accepted under the provisions of the Small Business Innovation Research Program.

RONJON ANNABALLI, 2D LT
Project Monitor, Material Process Design
Integration and Operations Division
Materials Directorate

STEVEN R. LECLAIR
Branch Chief, Material Process Design
Integration and Operations Division
Materials Directorate

MATTHEW DI BIASE, Maj, USAF
Deputy Chief, Integration and Operations Division
Materials Directorate

Publication of this report does not constitute approval or disapproval of the ideas or findings. It is published in the interest of scientific and technical information exchange.

Copies of this report should not be returned unless return is required by security considerations, contractual obligations, or notice on a specific document.

REPORT DOCUMENTATION PAGE

Public reporting burden for this collection of information is estimated to average 1 hour per response, including the time for reviewing instructions, searching existing data sources, gathering and maintaining the data needed, and completing and reviewing the collection of information. Send comments regarding this burden estimate or any other aspect of this collection of information, including suggestions for reducing this burden, to Washington Headquarters Services, Directorate for Information Operations and Reports, 1215 Jefferson Davis Highway, Suite 1204, Arlington, VA 22202-4302, and to the Office of Management and Budget, Paperwork Reduction Project (0704-0188), Washington, DC 20503.

1. AGENCY USE ONLY (Leave blank)	2. REPORT DATE	3. REPORT TYPE AND DATES COVERED
	January 1995	Final Report 1 Jul 94–31 Dec 94

4. TITLE AND SUBTITLE
Process Optimization Through Discovery and Integration of Materials and Processing Properties

5. FUNDING NUMBERS
C   F33615-94-C-5805
PE   65502F, 62102F
PR   3005
TA   09

6. AUTHOR(S)

Percy Yip

7. PERFORMING ORGANIZATION NAME(S) AND ADDRESS(ES)

AI WARE, Incorporated
1100 Cedar Avenue
Cleveland, OH 44106

8. PERFORMING ORGANIZATION REPORT NUMBER

9. SPONSORING / MONITORING AGENCY NAME(S) AND ADDRESS(ES)

Materials Directorate
Wright Laboratory
Air Force Materiel Command
Wright Patterson AFB, OH 45433-7734

10. SPONSORING / MONITORING AGENCY REPORT NUMBER

WL-TR-95-4019

11. SUPPLEMENTARY NOTES

This is a Small Business Innovation Research (SBIR) Report Phase 1

12a. DISTRIBUTION / AVAILABILITY STATEMENT

APPROVED FOR PUBLIC RELEASE; DISTRIBUTION IS UNLIMITED

12b. DISTRIBUTION CODE

13. ABSTRACT (Maximum 200 words)
The research objective is to examine process discovery methods for increasing the productivity of materials research with use of computational intelligence paradigms. Phase I work focused on the study of procedures and enabling technologies to achieve the ultimate goal. The overall work consists of four important tasks.

Task 1 was related to process modeling and monitoring. Once this task has been achieved, appropriate control actions can be generated based on an estimation of the current state of a process. In task 2, we focused our study on a feedforward/ feedback optimal control methodology with use of neural networks and evolutionary programming. Task 3 was an illustration how a pattern of film thickness estimated from task 1 could be used to formulate an objective function. With such an objective function, appropriate control actions can be generated via an optimal control software. Task 4 was concerned with development of an intelligent visualization display enabling users to understand and discover the process behavior.

14. SUBJECT TERMS
Evolutionary Programming, Processing, Optimization, QPA, Discovery, Modeling, Neural Networks, Control

15. NUMBER OF PAGES
20

16. PRICE CODE

17. SECURITY CLASSIFICATION OF REPORT	18. SECURITY CLASSIFICATION OF THIS PAGE	19. SECURITY CLASSIFICATION OF ABSTRACT	20. LIMITATION OF ABSTRACT
Unclassified	Unclassified	Unclassified	UL

I. Summary Of The Phase I Work

The research objective is to examine process discovery methods for increasing the productivity of materials research with use of computational intelligence paradigms. In particular, studies have been done on the self-directed control of growth of thin film structures with Molecular Beam Epitaxy (MBE) and Chemical Vapor Deposition (CVD) processes.

Phase I work focused on the study of procedures and enabling technologies to achieve the ultimate goal. The overall work consists of four important tasks as follows :

1. To investigate methods for on-line parameter interpretation of in-situ process-monitoring sensor data;
2. To investigate neural-network based optimal process control;
3. To illustrate how a pattern of film thickness can be interpreted to generate appropriate control actions for correcting non-uniformities in film thickness;
4. To investigate a memory and display methodology, called Visual Episodal Associative Memory, and to demonstrate that it can be used as an enabling technology for process discovery.

Task 1 was related to process modeling and monitoring. Once this task has been achieved, appropriate control actions can be generated based on an estimation of the current state of a process. In task 2, we focused our study on a feedforward/feedback optimal control methodology with use of neural networks and evolutionary programming. Task 3 was an illustration how a pattern of film thickness estimated from task 1 could be used to formulate an objective function. With such an objective function, appropriate control actions can be generated via an optimal control software. Task 4 was concerned with development of an intelligent visualization display enabling users to understand and discover the process behavior.

II. On-line Parameter Interpretation Of Sensor Data.

Survey was done in the interpretation of optical ellipsometry measurements during growth processes of multi-layer thin film structures of semiconductor materials with Molecular Beam Epitaxy (MBE) or Chemical Vapor Deposition (CVD) processes. The mathematical model of ellipsometry is based on Fresnel equations, that allows us to determine the values of ellipsometry measurements, given optical characteristics of the film and substrate, film thickness, wavelength and angle of incidence [1]. The ellipsometry measurements are two angles ψ and Δ, which define the ratio ρ of the complex-amplitude reflection coefficients R_p and R_s for the p and s polarizations. The corresponding equations are

$$\rho = \frac{R_p}{R_s} = \exp(j\Delta)\tan\psi \qquad (1)$$

1

$$\exp(j\Delta)\tan\psi = \rho\left(n_s, k_s, n_f, k_f, d_f, \lambda, \phi_0\right) \qquad (2)$$

Equation (2) gives a direct calculation of ψ and Δ given the optical characteristics of the substrate (n_s, k_s), of the film (n_f, k_f), the thickness of the film (d_f), the wavelength (λ) and the angle of incidence (ϕ_0). However, the optical charateristics of the film (n_f, k_f), thickness (d_f) are not directly measurable. Only the values of ellipsometry measurements (ψ and Δ) can be measured with process sensor. The interpretation of the ellipsometry measurement requires the inversion of the Fresnel equation. Such a direct inversion is impossible. However, using a sequence of ellipsometry measurements as indicated in Figure 1, it is possible to do such an inversion task. Possible methods include Newton's methods [2], multiwavelength (MW) and variable angle-of-incidence spectroscopic ellipsometry (VASE) techniques [3-5], multilayered neural networks [6] and Functional Link Nets (FLN) [7,8]. A survey of current works indicated that Park's method using FLN is efficient and capable of real-time interpretation [8]. The added advantage of using FLN is that the error function of the network is quadratic and so efficient learning methods such as conjugate learning method can be employed and global optimization is warranted [9]. Park divided the whole region of interest into many subregions, and a neural network is used to learn the mapping for each subregion. Highly accurate estimates as shown in Table 1 resulted from this divide-and-conquer method. It is one of the best current methods for parameter interpretation, but some comments on Park's current implementation need to be made here.

- In Park's work, a huge number of training patterns are required to train the neural network system if a high degree of accuracy is needed. It is reasonable because of the accuracy of a neural network is determined by the training set. We would like to mention the capability of AI WARE's existing CAD/CHEM software. It seems to us that the optimization capability of the CAD/CHEM software can indeed be utilized to get a highly accurate optical characteristics and film thickness, starting with initial values estimated from a trained Functional Link Net. With use of CAD/CHEM, we can reduce the requirement of a huge training set. The use of CAD/CHEM for the parameter interpretation will be tested in Phase II.

2

(Ψ_3, Δ_3)

(Ψ_2, Δ_2)

(Ψ_1, Δ_1)

(Ψ_0, Δ_0)
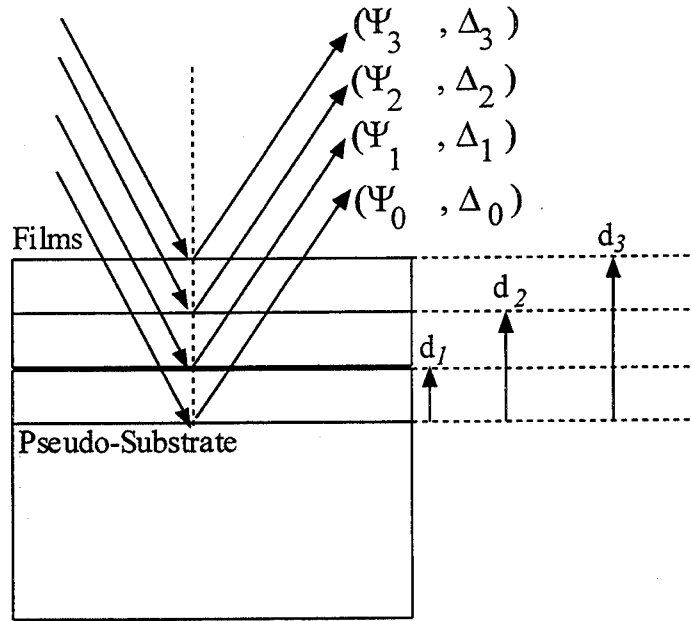
Films

Pseudo-Substrate

d_3 d_2 d_1

Figure 1 Schematic illustration of the sequence of measurements

Table 1 Actual and percentage errors in estimating film properties and depths using several subregion neural-nets

subregion	errors	n_1	k_1	d_1	d_2	d_3
3:6	actual	0.01128	0.00157	0.097	0.083	0.119
	percentage	0.268%	0.544%	0.587%	0.248%	0.232%
3:9	actual	0.00933	0.00122	0.064	0.094	0.157
	percentage	0.222%	0.422%	0.396%	0.277%	0.308%
3:10	actual	0.00778	0.00144	0.073	0.094	0.130
	percentage	0.185%	0.499%	0.434%	0.282%	0.258%
4:5	actual	0.00819	0.00128	0.093	0.113	0.144
	percentage	0.195%	0.453%	0.566%	0.331%	0.285%
5:9*	actual	0.00549	0.00174	0.345	0.371	0.444
	percentage	0.129%	0.610%	2.100%	1.089%	0.886%
6:9*	actual	0.00310	0.00208	1.046	1.022	1.016
	percentage	0.073%	0.761%	6.285%	3.035%	1.994%
7:5	actual	0.00451	0.00336	0.150	0.229	0.189
	percentage	0.106%	1.178%	0.852%	1.610%	0.377%
7:10*	actual	0.00229	0.00214	1.478	1.610	1.644
	percentage	0.054%	0.780%	9.218%	4.796%	3.256%

* in the subregions of (5:9), (6:9) and (7:10), the properties of pseudosubstrate approach to those of the homogenous (infinite thickness) film material (inside the subregion (7:10)). This is why the percentage errors of the depth estimates are large but the actual errors are in fact quite small.

We suggest that a hybrid method using a forward model (Fresnel's equation) and an inverse net should be used. The outputs of the inverse net provide an initial guess of optical characteristics and thickness of the film. Such an initial estimate can be optimized using CAD/CHEM to provide a more accurate result. Using such a hybrid scheme, a

3

coarsely trained neural network may be sufficient to provide initial estimates of the optical characteristics and thickness of the film.

III. Self-Directed Control With Use Of Feedforward/Feedback Control

Here, we will discuss our study on the use of feedforward and feedback control methodologies. In general, control methodologies can be classified as feedforward (open-loop) or feedback (closed-loop). The advantages of using feedback control are well understood as follows :
- it can reduce system error;
- it is insensitive to external disturbances and internal variations of system parameters.

Since a feedback system is insensitive to parameter variation and noise, it is possible to control a process in a fairly good manner even the system model is not exact. The benefit of using feedback control methodology is that we don't need a very accurate system model. However, the use of feedback control may introduce instability problem, that arise when the system tends to overcorrect errors that may cause oscillation.

Though feedforward (or open-loop) control is not taken as an advanced control methodology by itself, there are still many advantages of using it, namely :
- stability can easily be assured;
- planning a sequence of control actions is possible.

Feedforward control is very sensitive to parameter variations and external disturbances, but the system can easily be assured to be stable. Feedback control systems, on the other hand, have the advantages when unpredictable disturbances and unpredictable variations of system parameters occur. Hence a proper combination of feedforward and feedback control is desirable.

AI WARE's FLN Control Toolkit is a version of feedforward and feedback learning control software. The block diagram is shown in Figure 2. It combines the advantages of feedforward control, feedback control and the learning capability of neural networks. Optimal control can also be achieved with the use of GESA [10,11], a version of evolutionary programming. Feedback control is implemented via PID, as PID is quite an industrial standard. The use of feedforward control enables us to tune the PID gains in the optimal manner according to users' objectives.
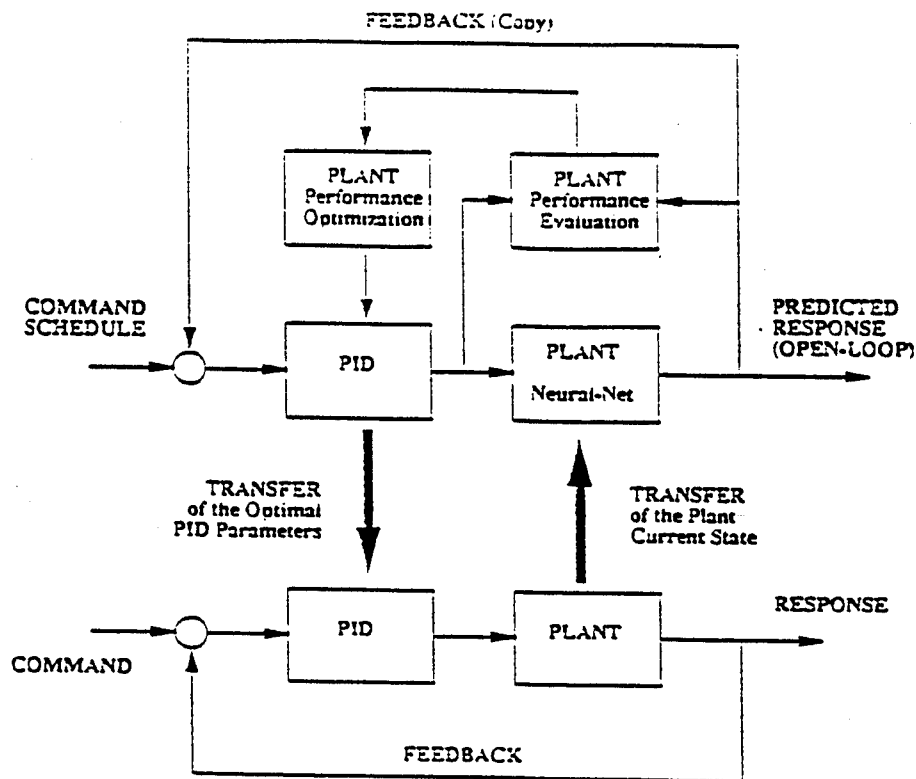
Figure 2. A version of optimal control implementation with use of optimization

We illustrate the benefit of optimal control with use of FLN Control Toolkit with Figures 3-5. The process that we used was a second-order time-invariant process with external disturbance added to the system periodically. As illustrated in Figure 3, PID gains were set constant during the whole course of control process. the system was a standard feedback control system and was able to return back to the set point slowly. We can also minimize a user-defined objective as illustrated in Figure 4, and Figure 5. During optimal control tuning process, the system makes use of the open-loop predictive capability of the neural network model to determine the optimal values of the PID gains so as to achieve the user-defined objective. Figure 4 illustrate the responses and the control actions when the objective was to minimize the sum of the square of the deviation from the set point and the square of the control actions. Figure 5 illustrate the responses and the control actions when the objective was to minimze the sum of the square of the deviation from the set points and the square of the rate of change of control actions. Both Figures 4 and 5 indicate that the system returned to the set point quickly because the

deviation from the set point was part of the objective. The control action was smooth in Figure 5 because it was part of the objective as well.
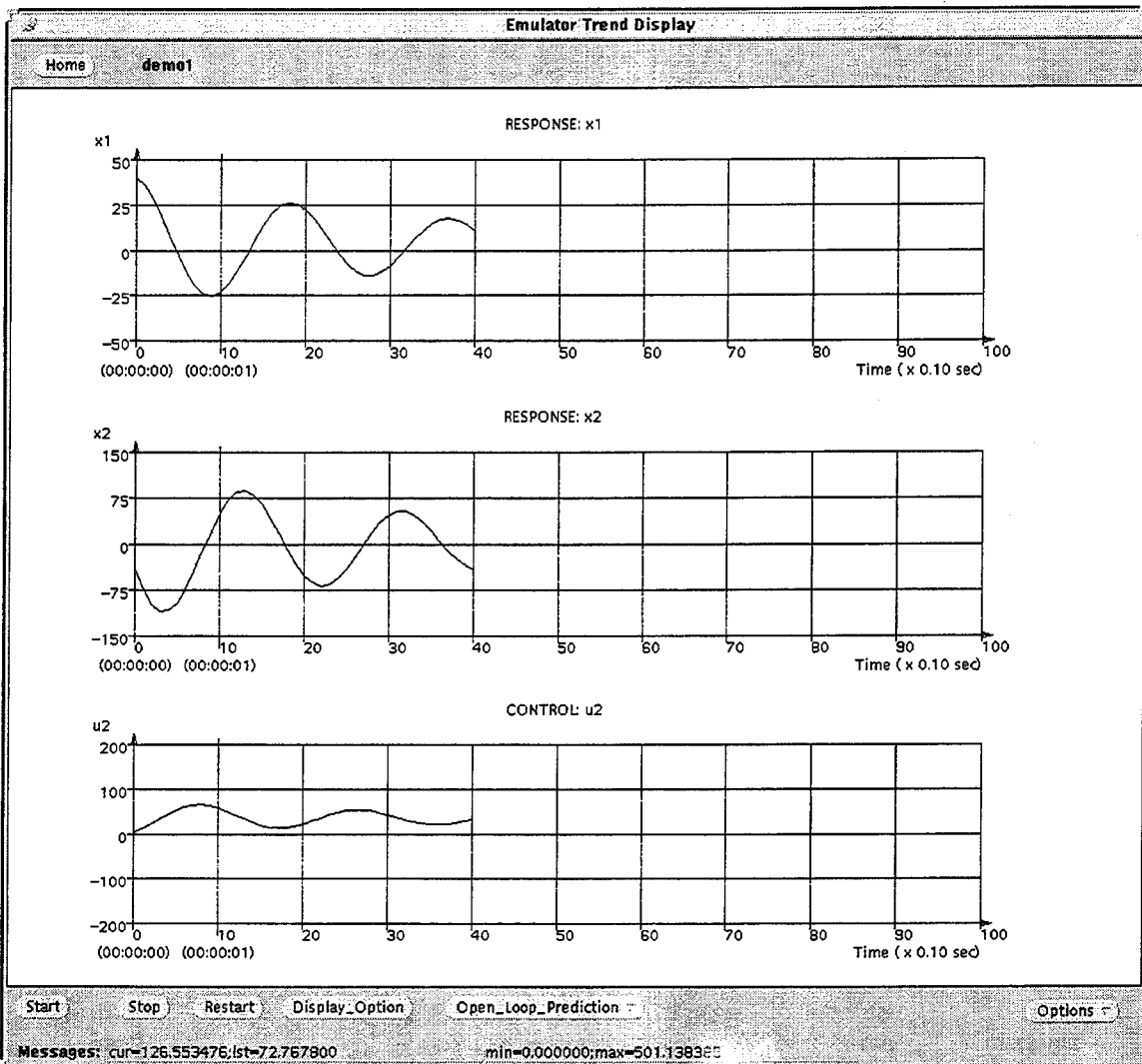

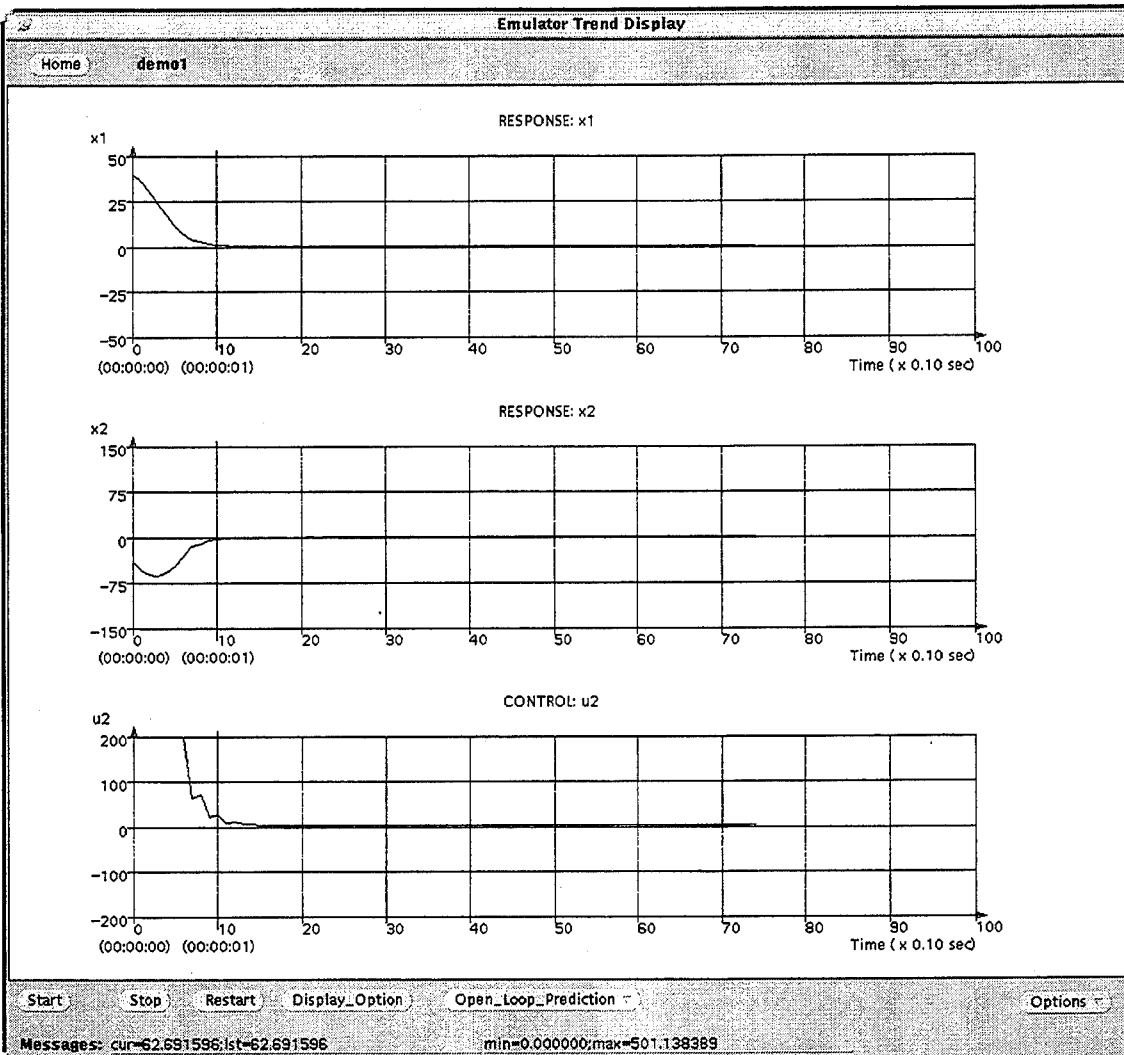Figure 3 Illustration of system response with use a constant PID controller

Figure 4 Optimal system response with optimal PID gains tuned with GESA to minimize the output deviation as well as the input power
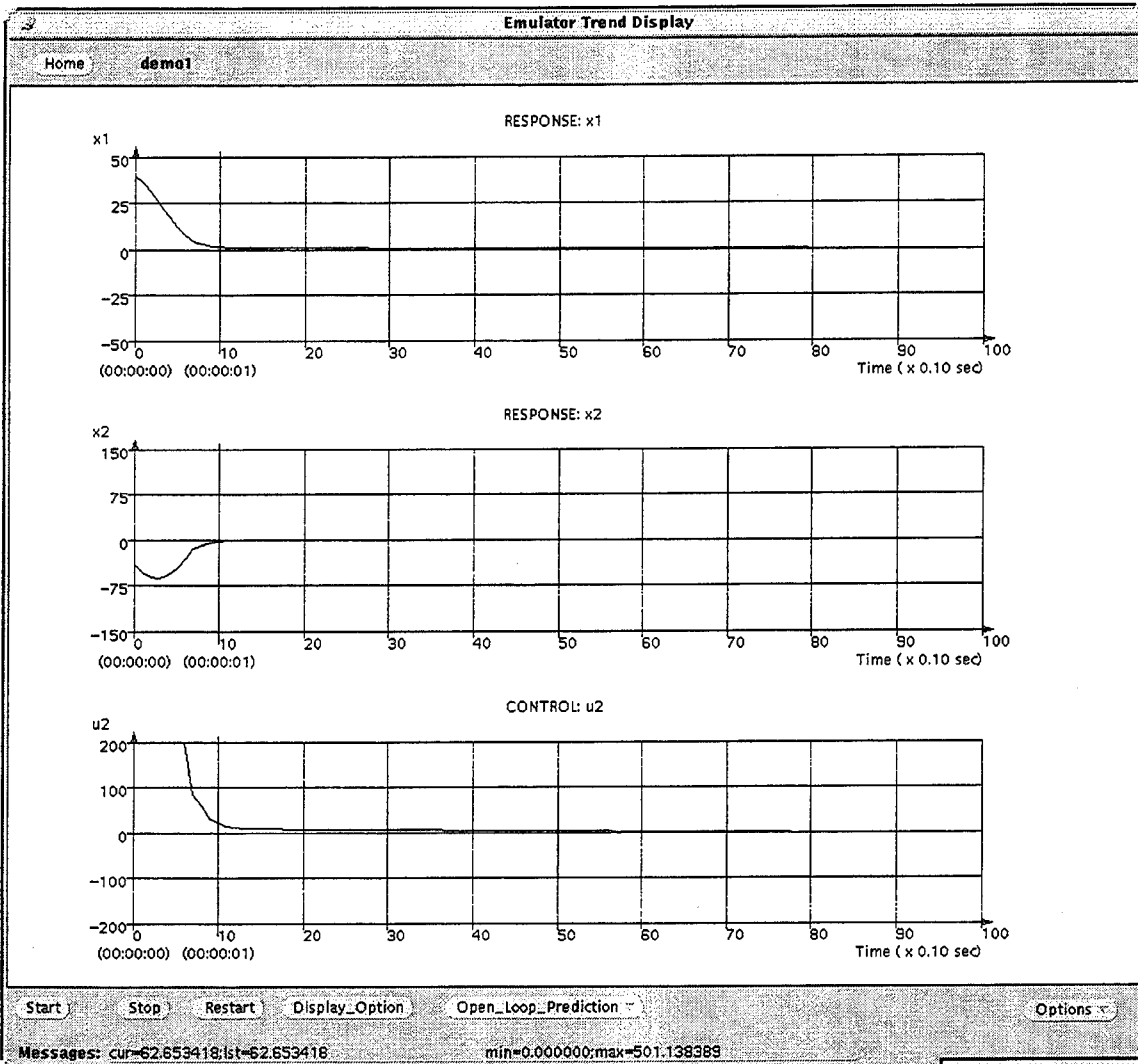
Figure 5 Optimal system response with optimal PID gains tuned with GESA to minimize the output deviation as well as the rate of change of control input

The benefit of FLN Control Toolkit can be summarized as follows :
- it is a learning and adaptive control;
- it is a combination of feedforward and feedback control;
- optimal control can be achieved through the use of objective functions;
- objective functions can be dynamically changed to suit current operating conditions.

IV. Interpretation Of Film Thickness Data

A pie shaped aperture correctly positioned over a rotating substrate would yield a uniform film (Fig.6-a). This is not the case if the aperture is misplaced (Fig.6-b, Fig.6-c).
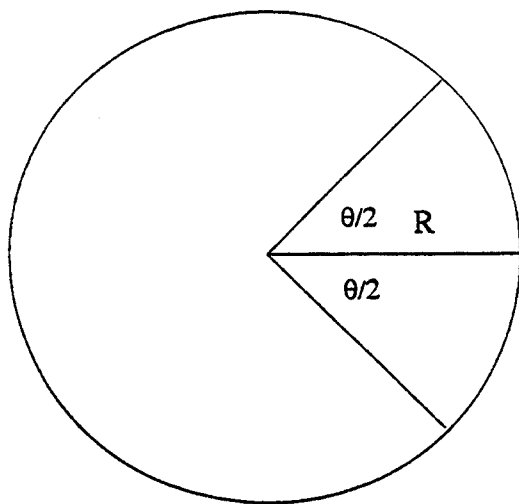
(a) Depiction of Pie-Shaped Aperture Centered Accurately With Respect to Rotating Aperture
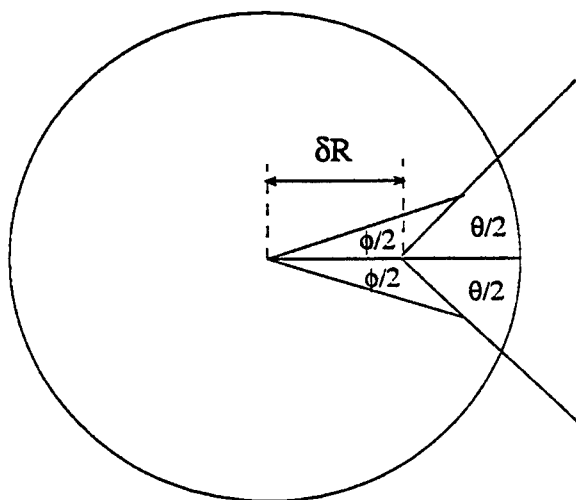
(b) Depiction of Geometry of Radially Displaced Aperture

(c) Depiction of Geometry of Tilted Aperture

Figure 6 Geometry of Possible Misalignments
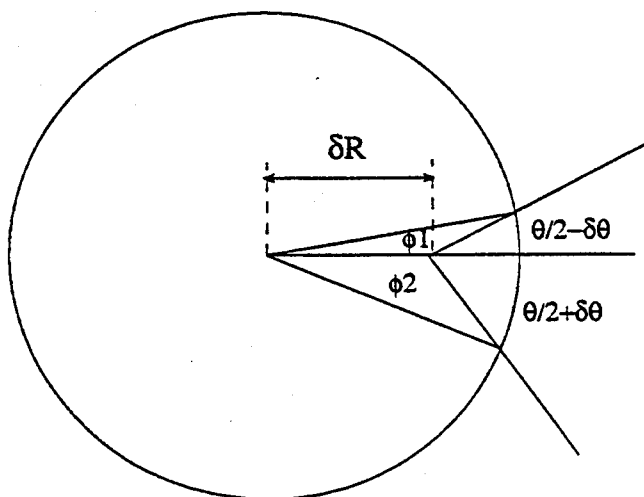
Misplacement is determined by the two parameters δR, linear displacement, and $\delta\theta$, angular displacement, as shown in Fig.6-c. The value of the angular displacement $\delta\theta$ can be restricted to satisfy the condition $0 \leq \delta\theta \leq \theta/2$, which is realistic restriction. The thickness of the film per one revolution $d(r)$ at any point of the circumference of radius r, $0 \leq r \leq R$ depends on the value of the time which the point spends, traveling inside the aperture. That latter value is proportional, assuming uniform rotation of the substrate, to the value of the angle $\phi = \phi_1 + \phi_2$. Therefore,

$$d(r) \propto \phi_1 + \phi_2.$$

The simplest case and perhaps one of the more important cases is that when that the center of the circle of radius R (center of rotation of the substrate) is outside of the aperture. For that circumstance the circumference of radius r intersects both of the linear sides of the pie, each side at one point. It is obtained that the thickness would vary with the radial position r in the following manner.

$$d(r) \propto \begin{cases} \theta - \arcsin\left[\dfrac{\delta R}{r}\sin(\theta/2+\delta\theta)\right] - \arcsin\left[\dfrac{\delta R}{r}\sin(\theta/2-\delta\theta)\right], & \delta R \leq r \leq R \\ 0, & 0 \leq r \leq \delta R \end{cases} \tag{3}$$

Graphs of $d(r)$ vs. r are shown in Fig. 7 for different values of δR and $\delta\theta$.

Expression (3) is valid for all cases where the center of the sunstrate is outside of the aperture. Formulas for $d(r)$ for cases with the center of the substrate within the aperture have also been derived and are exibited in Fig. 8 with the aid of some explanatory illustrations at the end of this discussion.

In practice, given a number of measurements of the thicknesses $d_1, d_2, ... d_N$ for points situated at the distances $r_1, r_2, ... r_N$ from the center the substrate, estimates of the corrective control actions $\delta R, \delta\theta$, which will restore the aperture to the correct relative position, can be obtained. The correct control actions are generated by minimizing the error function

$$F(\delta R, \delta\theta) = \sum_{n=1}^{N}\left[d_n - d(r_n)\right]^2, \tag{4}$$

where $d(r_n)$, $n = 1, ... N$ are calculated using expressions (3) or (5). The desired values δR and $\delta\theta$ are those which bring the function F to the minimum. Minimization can be done using different efficient stochastic guided procedures such as GESA [12] or SOPT [13]. In practice, for visualization purposes, three-dimensional profiles of the film could be displayed for successively more accurate estimates of the control actions δR and $\delta\theta$ as control progresses.

For the case when the center of the substrate is inside of the aperture it is convenient to divide the aperture into 6 subregions and to represent ϕ as the sum of 6 angles $\phi_1, \phi_2, ... \phi_6$, where ϕ_i is part of ϕ lying within subregion i, $i = 1, ... 6$ (See Fig. 8).
Values of $R_1, ... R_6, \theta_1, ... \theta_6$ are determined by the relative positions of the aperture and the substrate and are independent of the variable r. Their values can be successively precalculated by the following formulas

10

$$R_2 = \delta R, \quad R_5 = R - \delta R, \quad \theta_1 = \theta/2 - \delta\theta, \quad \theta_2 = \theta/2 + \delta\theta, \quad R_1 = R_2 \sin\theta_1, R_3 = R_2 \sin\theta_2$$
$$R_4 = \sqrt{R^2 + R_2^2 - 2RR_2 \cos\theta_2},$$
$$R_6 = \sqrt{R^2 + R_2^2 - 2RR_2 \cos\theta_1}, \tag{5}$$
$$\theta_3 = \arcsin\frac{R_3}{R_4}, \quad \theta_4 = \theta_2 + \theta_3, \quad \theta_6 = \arcsin\frac{R_1}{R_6}, \quad \theta_5 = \theta_1 + \theta_6.$$

The thickness is given by the following formula

$$d(r) \propto \sum_{i=1}^{6} \phi_i, \tag{6}$$

where

$$\phi_1 = \begin{cases} 0, & r \geq R_2 \\ \arcsin\left(\dfrac{R_2}{r}\sin\theta_1\right) - \theta_1, & R_1 \leq r \leq R_2, \\ \pi/2 - \theta_1, & 0 \leq r \leq R_1 \end{cases}$$

$$\phi_2 = \begin{cases} 0, & r \geq R_2 \\ \arcsin\left(\dfrac{R_2}{r}\sin\theta_2\right) - \theta_2, & R_3 \leq r \leq R_2 \\ \pi/2 - \theta_2, & 0 \leq r \leq R_3 \end{cases}$$

$$\phi_3 = \begin{cases} 0, & r \geq R_4 \\ \arcsin\left(\dfrac{R_4}{r}\sin\theta_3\right), & R_3 \leq r \leq R_4, \\ \pi/2 - \theta_3, & 0 \leq r \leq R_3 \end{cases}$$

$$\phi_4 = \begin{cases} 0, & r \geq R_4 \\ \theta_4 - \arccos\left[\dfrac{R^2 - r^2 - R_2^2}{2rR_2}\right], & R_5 \leq r \leq R_4, \\ \theta_4, & 0 \leq r \leq R_5 \end{cases}$$

$$\phi_5 = \begin{cases} 0, & r \geq R_6 \\ \theta_5 - \arccos\left[\dfrac{R^2 - r^2 - R_2^2}{2rR_2}\right], & R_5 \leq r \leq R_6, \\ \theta_5, & 0 \leq r \leq R_5 \end{cases}$$

$$\phi_6 = \begin{cases} 0, & r \geq R_6 \\ \arcsin\left(\dfrac{R_4}{r}\sin\theta_6\right), & R_1 \leq r \leq R_6. \\ \pi/2 - \theta_6, & 0 \leq r \leq R_1 \end{cases}$$
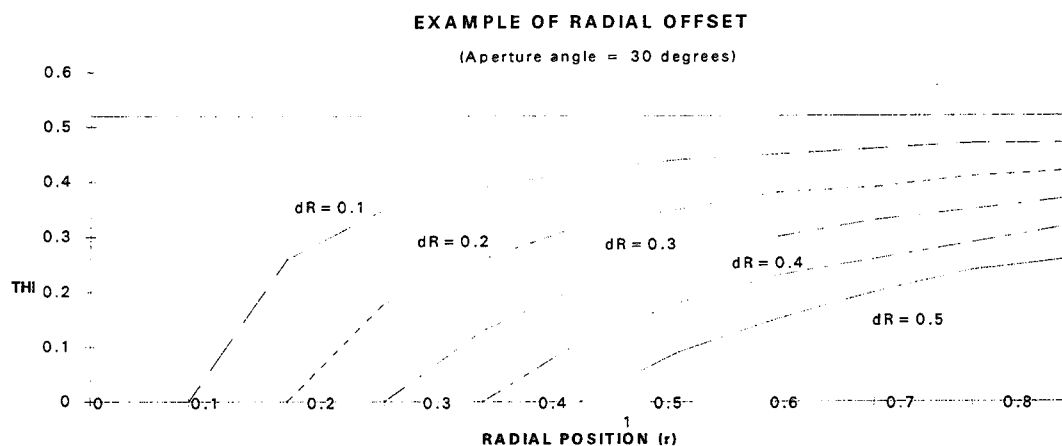
EXAMPLE OF RADIAL OFFSET

(Aperture angle = 30 degrees)

Figure 7a Effective of Radial Misalignments (δR) on Thickness Profiles

EXAMPLE OF ANGULAR OFFSET
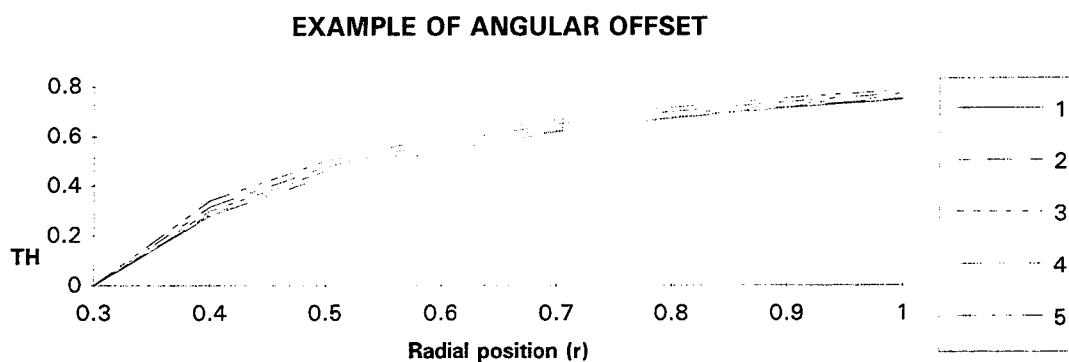
Figure 7b Effective of Angular Misalignments ($\delta\theta$) on Thickness Profiles
All graphs are drawn for $R = 1$, $\delta R = 0.3$, $\theta = \pi / 3$
Curve 1 corresponds to $\delta\theta = \pi / 30$, curve 2 corresponds to $\delta\theta = \pi / 15$, curve 3 corresponds to $\delta\theta = \pi / 10$, curve 4 corresponds to $\delta\theta = 2\pi / 15$ and curve 5 corresponds to $\delta\theta = \pi / 6$

Figure 7 Illustration of the effect of Misalignments

Figure 8 Schematic illustration of the subregions

12

V.   Visual EAM: An Intelligent Visualization Tool For Discovery

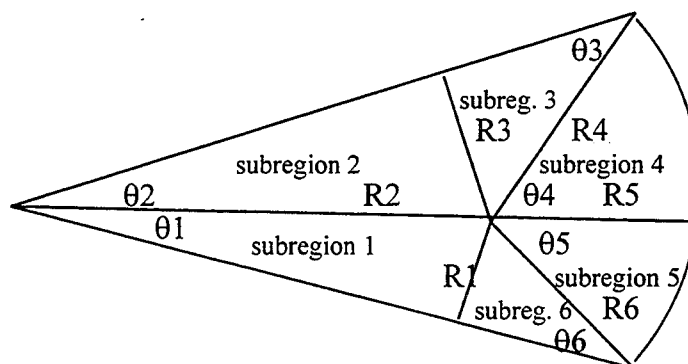Visual Episodal Associative Memory (Visual EAM) is a powerful intelligent visualization tool developed by AI WARE. Though it is not so directly related to process control, it is very important by itself in the context of discovery. The idea of Visual EAM is that of projecting high-dimensional objects into two-dimensional space in a manner that meaningful information can be extracted and visualized. In this report, we will describe some of the usages of Visual EAM.

Table 2 List of objects

Label	Original Attributes					Transformed Coordinates	
	a1	a2	a3	a4	a5	x	y
A	1	0	0	0	0	0.999508	0.999562
B	2	0	0	0	0	0.999506	0.999557
C	3	0	0	0	0	0.999503	0.999551
D	4	0	0	0	0	0.999498	0.999544
E	5	0	0	0	0	0.999492	0.999535
F	3	1	0	0	0	0.714601	0.648197
G	3	2	0	0	0	0.469410	0.354227
H	3	3	0	0	0	0.455890	0.271452
I	3	4	0	0	0	0.972253	0.060956
J	3	5	0	0	0	0.999640	0.001557
K	3	3	1	0	0	0.388928	0.224456
L	3	3	2	0	0	0.337869	0.182086
M	3	3	3	0	0	0.298414	0.143284
N	3	3	4	0	0	0.257642	0.109643
O	3	3	5	0	0	0.220664	0.070379
P	3	3	6	0	0	0.201904	0.040221
Q	3	3	7	0	0	0.198844	0.017906
R	3	3	8	0	0	0.204662	0.000990
S	3	3	3	1	0	0.218765	0.177039
T	3	3	3	2	0	0.168311	0.197174
U	3	3	3	3	0	0.116724	0.215950
V	3	3	3	4	0	0.046178	0.245005
W	3	3	6	1	0	0.143387	0.083768
X	3	3	6	2	0	0.103514	0.116506
Y	3	3	6	3	0	0.067075	0.147464
Z	3	3	6	4	0	0.024474	0.184802
1	3	3	6	2	1	0.084070	0.095475
2	3	3	6	2	2	0.066193	0.076672
3	3	3	6	2	3	0.050128	0.059229
4	3	3	6	2	4	0.034308	0.042277
5	3	3	6	2	5	0.017574	0.023258
6	3	3	6	2	6	0.000572	0.000668

Consider a list of objects with five attributes as illustrated in Table 2 [14]. These objects are labeled A,B,C,....,1,2,3,4,5,6. There is no special meaning attached to these labels. Each of the objects is described in terms of the values of their five attributes. These objects can be transformed nonlinearly into a two-dimensional space using Visual EAM. It is clearly impossible to display all the information contained in a five-dimensional space relationship in a two-dimensional display, but it is possible to devise a meaningful display, curtailed and abstracted but nevertheless convenient and suitable for many purposes. A display obtained with Visual EAM is shown in Figure 9.
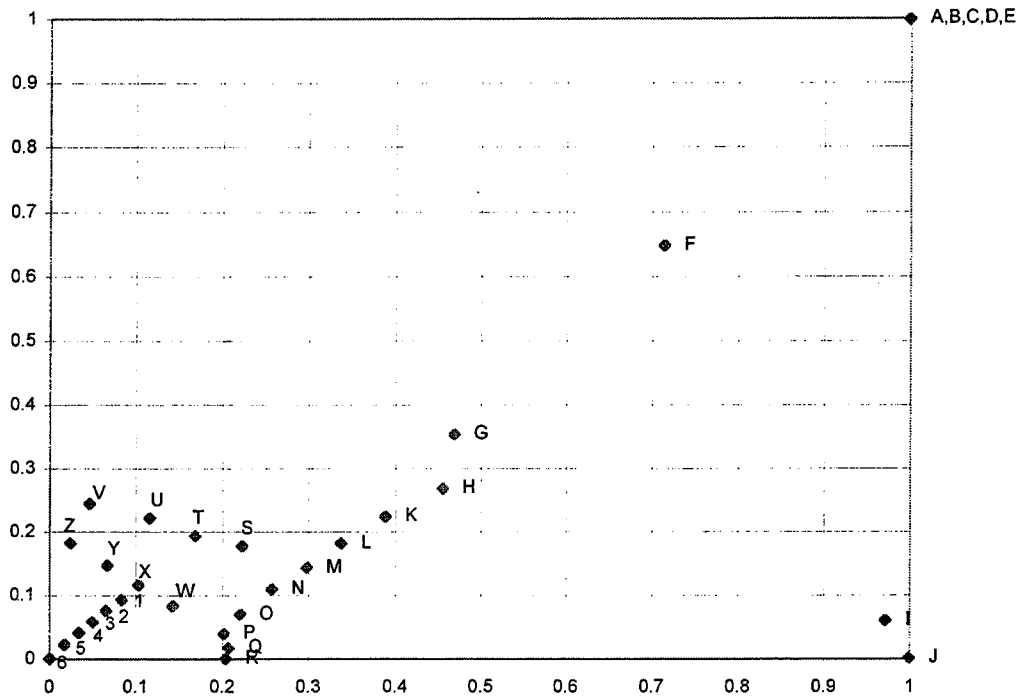
(a)
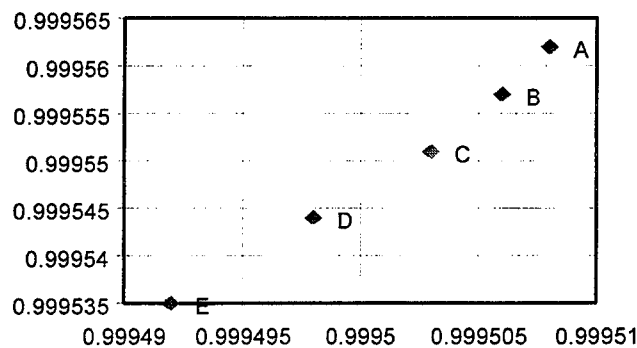
(b)

Figure 9 Two-dimensional display of the objects obtained with Visual EAM:
(a) in normal 0 to 1 scale; (b) with zoom-in of the top right corner

14

It is seen that objects which are close in five-dimensional space are also close in this two dimensional display. The objects A,B,C,D,and E are all squashed at the upper right-hand corner of Figure 9. However, zooming in onto that part of the display, it may be observed that the five objects are apart but very close to each other. Examining the values of the attributes in Table 2 shows that it is reasonable and informative.

As an illustration of a use of such a display consider the task of exploring the question of what objects have high values in the third attribute and those which have high values in the fourth attribute. The intersection of the two separate distributions is readily observed as illustrated with Figure 10. This is a simple illustration of the many different ways in which this interesting display can be utilized.
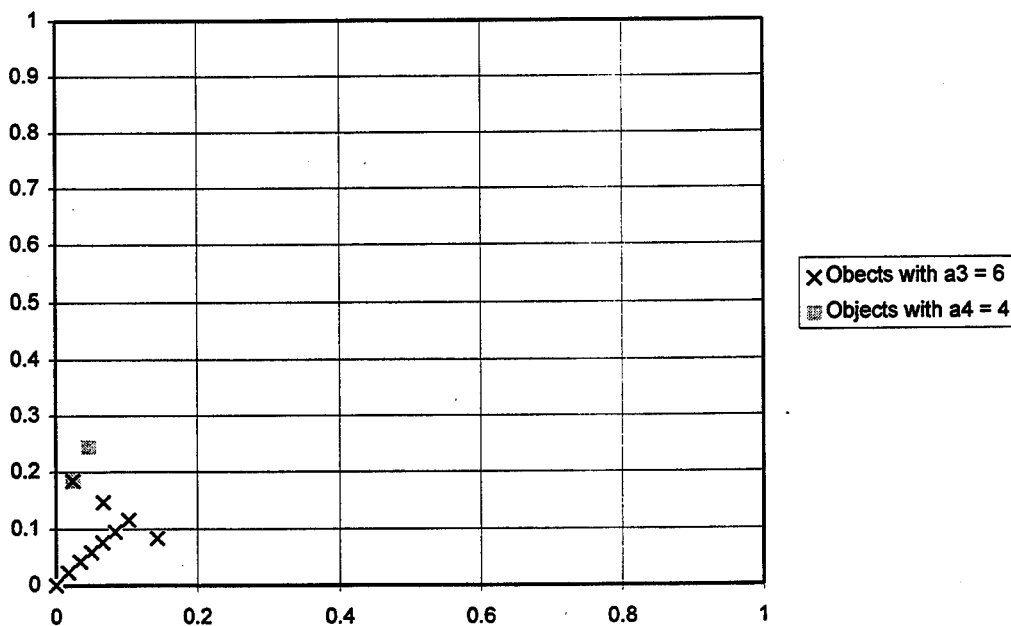

Figure 10 Illustration of the usage of Visual EAM for discovery of relationship of the attributes

Investigation also has been done on the use of Visual EAM for categorization and rule discovery. To demonstrate that, we used a gasoline blending task [15] as an example. The set of the training data is shown in Table 1. The task of the blending problem is to find out what combinations of the input ingredients provide a high octane amount of over 100 (class = 1). It has been demonstrated by CWRU that it is impossible to find out the proper clusters using K-means or other unsupervised learning methods. We used a version of Visual EAM and found out that the two classes are indeed able to be separated, as illustrated in Figure 11. The high octane class was found to locate at the top-left corner of the two-dimensional map, whereas the low octane class was located at the bottom-right corner.

Table 3 List of training set for gasoline blending task

| a1 (Butane)	a2 (Isopenetane)	a3 (Reformate)	a4 (CatCracked)	a5 (Alkylate)	Class
0	0	0.35	0.6	0.06	1
0	0.3	0.1	0	0.6	1
0.15	0	0.15	0.6	0.1	0
0	0.3	0.049	0.6	0.051	0
0.15	0.127	0.023	0.6	0.1	0
0	0.158	0.142	0.1	0.6	1
0.067	0.098	0.234	0.332	0.27	1
0	0.126	0.174	0.6	0.1	0
0.075	0	0.225	0.6	0.1	0
0	0.3	0	0.1	0.6	1
0.15	0.15	0.1	0.6	0	0
0	0.3	0	0.489	0.211	0
0.15	0	0.311	0.539	0	0
0	0.3	0.285	0.415	0	0
0	0.08	0.35	0.57	0	1
0.15	0.15	0.266	0.434	0	0
0.15	0.15	0.082	0.018	0.6	1
0	0	0.3	0.461	0.239	1
0.15	0.034	0.116	0.1	0.6	1
0.068	0.121	0.175	0.444	0.192	0
0	0.3	0.192	0.208	0.3	1
0.15	0.15	0.174	0.226	0.3	1
0.075	0.225	0.276	0.424	0	0
0.075	0.225	0	0.1	0.6	1
0.15	0.15	0	0.324	0.376	0
0	0.3	0.192	0.508	0	0
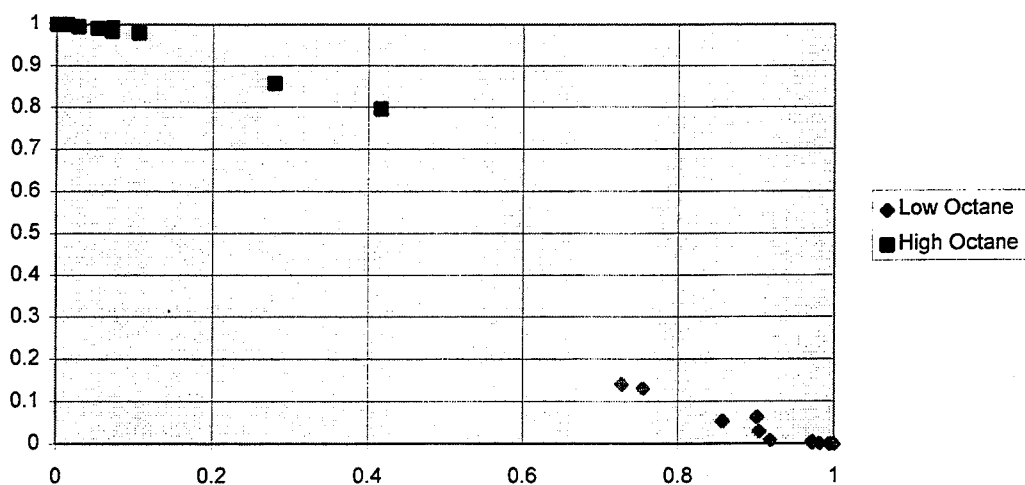
Figure 11 Illustration of separation of two classes with use of Visual EAM

To further discover the relationship of the process, we pointed to the memory points in the map and the original input ingredients were revealed. Investigation of some of the memory points in the map indicated that a5 (Alkylate) is high. A hypothesis like "if Alkylate is high, the octane should be high" naturally comes to our mind. This hypothesis can easily be verified with the associative memory capability of the Visual EAM. We used the association mode to display all the data with a5 > 4. The display is shown in Figure 12. It is clearly that the hypothesis is true for the training set. The negation of the hypothesis then became the second hypothesis. That is "if Alkylate is low, octane level should be low". Visual EAM displayed the memory points with low Alkylate (say a5 <= 4) as shown in Figure 13. Clearly the second hypothesis is not true. We then revealed the points and we continued the steps, we got the following qualitative rules:

- If a5 is high, octane level is high.
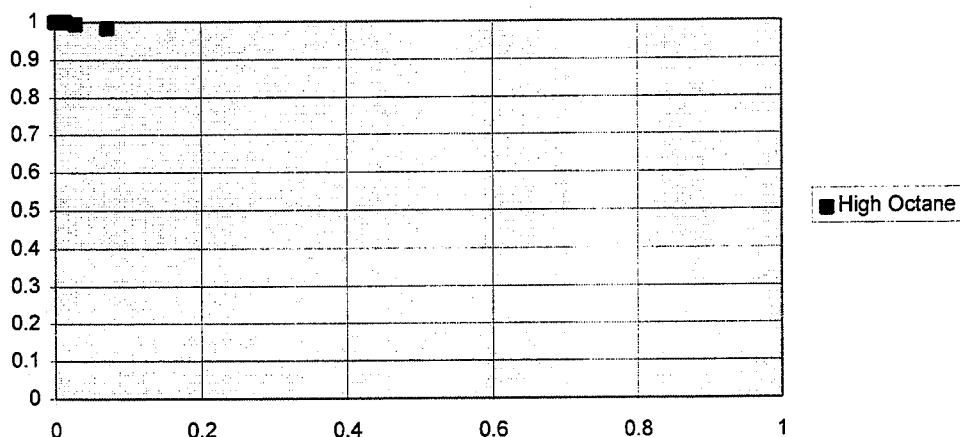- If a5 is medium, and a3 is high and a4 is high, octane level is high.
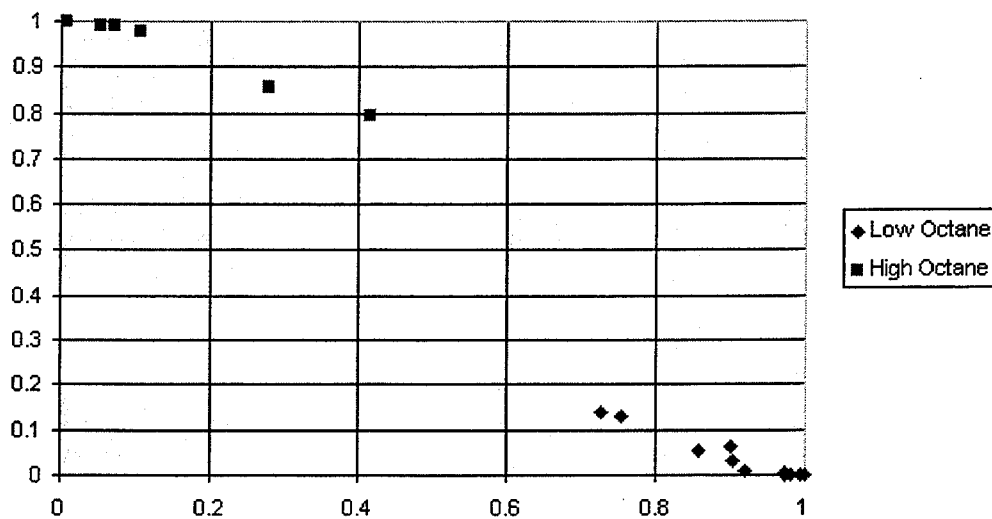

Figure 12 Display of all memory points with a5 > 4

Figure 13 Display of all memory points with a5 <= 4

This is a simple illustration of a man-machine interaction for process discovery. Hypothesis and questions are stimulated and generated with a display supported by Visual EAM. These hypothesis can be verified using the associative memory capability of Visual EAM. Another display is then generated and may stimulate other hypothesis. This is another usage of Visual EAM for rule discovery.

Another comment should be made here to indicate the potential of Visual EAM. We demonstrated one of many different procedures for man-human interaction for rule discovery. Since it is a simple 2-D display, we are confident that these rule discovery procedures can be automated. The potential integration of Visual EAM with Air Force's Qualitative Process Automation (QPA) will provide a powerful tool for process discovery and automation.

VI. Conclusion

Phase I has investigated the necessary components for process discovery and procedures for automation to increase the productivity of materials research. It has been verified that the method demonstrated by Park is efficient and capable of interpretation of ellipsometry measurements. AI WARE's FLN control toolkit has demonstrated the capability of learning a model, and controlling the process in the optimal manners. Analysis has been done to verify that misplacement of aperture in a MBE process can be detected and adjusted back to the proper position with thickness data. The development of Visual EAM provides a powerful tool for process discovery and automation.

In conclusion, Phase I has demonstrated that process discovery and automation can be done with an integration of advanced technologies in neural networks, evolutionary programming, learning control, and intelligent visualization tools.

References

[1] R. M. A. Azzam and N. M. Bashara. *Ellipsometry and Polarized Light*. Amsterdam: North-Holland, 1986.

[2] F. L. McCrackin, F. L. Panaglia, R. Stromberg, and H. S. Steinberg, "Measurement of the thickness and refractive index of very thin film and the optical properties of surfaces by ellipsometry," *Journal of Research of NBS*, **67A**, pp. 363-377, 1963

[3] S. A. Alterovitz, G. H. Bu-Abbud, J. A. Woollam, D. C. Liu, "An enhanced sensetivity null ellipsometry technique for studying films on substrate: Application to silicon nitride on gallium arsenide," *Journal of Applied Physics*, **54**, pp. 1559-1569, 1983.

[4] S. A. Alterovitz, J. A. Woollam, and P. G. Snyder. "Variable angle spectroscopic ellipsometry," *Solid State Technology*, **31**, Iss. 3, pp. 99-102, 1988.

[5] J. A. Woollam, P. G. Snyder, H. Yao, and B. Johs, "In-situ and ex-situ ellipsometric characterization for semiconductor technology," *SPIE*, **1678**, pp. 246-253, 1992.

[6] F. K. Urban, D. C. Park, and M. F. Tabet, "Development of artificial neural networks for real time, in-situ ellipsometry data reduction, *Thin Solid Films*, **220**, pp. 247-253, 1992.

[7] G. H. Park, Y. H. Pao, K. G. Eyink, S. R. Leclair, and M. S. Soclof, "Neural-net based optical ellipsometry for monitoring groeth of semiconductor films," *to appear in IFAC Publications,* Artificial Intelligence in Real-Time Control, 3-5 October 1994, Valencia, Spain.

[8] G. H. Park, Y. H. Pao, B. Igelnik, K. G. Eyink, and S. R. Leclair, "Neural-net computing for interpretation of semiconductor film optical ellipsometry parameters," *to appear in IEEE Transactions on Neural Networks.*

[9] Y.-H. Pao, G. H. Park, and D. J. Sobajic, "Learning and generalization characteristics of the random vector Functional-Link net," *Neurocomputing*, **6**, pp.163-180, Elsevier Press, 1994.

[10] P.P.C. Yip and Y.H. Pao, "Combinatorial optimization with use of guided evolutionary simulated annealing," *to appear in IEEE Transactions on Neural networks.*

[11] P.P.C. Yip and Y.H. Pao, "A guided evolutionary simulated annealing approach to the quadratic assignment problem," *IEEE Transactions on Systems, Man, and Cybernetics*, vol. 24, no. 9, Sept.,1994, pp. 1383-1387.

[12] P.P.C. Yip and Y.H. Pao, "A guided evolutionary computation technique as function optimizer," *Proceedings of the First IEEE Conference on Evolutionary Computation*, Orlando, Florida, June 26-July 2, 1994, pp. 628-633.

[13] B. Igelnik, Y.-H. Pao, "A stochastic optimization algorithm," *submitted to The Eighth International Conference on Industrial & Engineering Applications of Artificial Intellingence & Expert Systems*, Melbourne, June 5-9, 1995.

[14] T. Kohonen, "The self-organizing map," *Proceedings of the IEEE*, vol. 78, No.9, 1990, pp. 1464-1480.

[15] D.B. Fogel, L.J. Fogel and V.W. Porto, "Evolving neural networks," *Biological Cybernetics*, vol. 63, 1990, pp. 487-493.